Effect of enrichment functions on GFEM solutions of time-dependent conduction heat transfer problems

M. Iqbal[a,b,*], K. Alam[c], H. Gimperlein[d], O. Laghrouche[a], M.S. Mohamed[a]

[a] *Institute for Infrastructure and Environment, Heriot–Watt University, Edinburgh, EH14 4AS, United Kingdom*
[b] *Creative Engineering and Management Services, Deans Centre Peshawar, Pakistan*
[c] *Department of Mechanical and Industrial Engineering, College of Engineering, Sultan Qaboos University, Oman*
[d] *Maxwell Institute for Mathematical Sciences and Department of Mathematics, Heriot–Watt University, Edinburgh, EH14 4AS, United Kingdom*

Abstract

This article investigates the effect of the selection of enrichment functions on the formulation of the Generalized Finite Element Method (GFEM) for the solutions of transient heat conduction problems. We present the study of an *a-posteriori* error estimate with the aim to show it is a reliable tool for the selection of enrichment functions to efficiently capture the sharp thermal gradients of the solutions. Problems in two- and three-dimensional domains are considered to demonstrate the robustness of the proposed error estimate. Numerical experiments consider two different types of enrichment functions that mimic the solution behaviour and capture the time-varying thermal gradients. The presented study shows that the error estimate is independent of the heuristically selected enrichment functions and can be used for any type of enrichment functions. It is concluded that the proposed error estimate efficiently reflects the errors in the GFEM solutions for both types of enrichment functions and can be used as an effective tool for the selection of more suitable enrichment functions that produce lower errors under the considered thermal conditions.

Keywords: GFEM, *a-posteriori* error estimate, enrichment functions, conduction heat transfer

1. Introduction

The advent of domain based enrichment methods like the Partition of Unity Finite Element Method (PUFEM)[1] and partition of unity based generalized finite element method (GFEM)[2] and eXtended Finite Element Method (XFEM)[3] has attracted the attention of a large number of researchers in the last two decades. These methods are developed to reduce the meshing requirements and facilitate efficient simulation of complex problems with singularities. Repre-

*Corresponding author
Email address: iqbal@cemsglobal.org (M. Iqbal)

sentative examples include problems in solid mechanics [3, 4], multiphase flows [5], fluid structure interaction [6] and thermal problems with sharp gradients [7–9], among many others. The formulation of enriched finite element methods relies on the fusion of specially designed functions into the approximation space. These special functions, or enrichment functions, incorporate *a-priori* information about the solution of the considered problem. A suitable enrichment function approximates the solution better than the standard polynomial based shape functions. In fact, the accuracy of an enriched finite element method relies on the proper selection of enrichment functions [10]. Babuška and Banerjee [11] mentioned that the accuracy of GFEM solutions depends on the choice of enrichment functions. Strouboulis et al. [12] also showed that the choice of enrichment functions has an effect on the solutions of the GFEM formulation. They used polynomial and exponential enrichment functions to solve one-dimensional convection-diffusion problems. Turner et al. [13] also presented several enrichment functions for the solution of advection–difusion problems in one-dimensional domains. Some examples of suitable enrichment functions for specific applications can be found in [14].

In an ideal scenario, the enrichment functions should comprise the asymptotic solution space or represent the solution of the considered partial differential equation. In wave propagation problems, for example, the enrichment functions are taken from the exact solution of the problem. To solve Helmholtz and elastic wave problems, the wave potentials are expressed as linear combinations of plane waves which are known to be the solution of the underlying PDEs. This idea has been utilized for the solution of potential problems using PUFEM [15–18], GFEM [19–21], boundary element methods [22, 23], discontinuous Galerkin methods [24–26] and ultraweak variational formulations [27–29]. A similar idea has also been presented in the context of XFEM [3, 30] for fracture mechanics problems. The enrichment functions in XFEM are taken from the asymptotic solution space and are used to capture singularities around a crack tip [4]. Similar enrichment functions have also been used for modelling crack propagation using meshless [31] and boundary element methods [32, 33]. Aquino et al. [34] generated enrichment functions for GFEM using experimental and simulated data and used the Proper Orthogonal Decomposition (POD) technique.

Other enrichment techniques may include functions that do not represent the exact solution but somehow approximate the solution of the problem. An intuitive knowledge can be used to form enrichment functions that are not necessarily solutions of the underlying PDEs of the considered problems. This is particularly helpful for problems where no exact solution space is available. Mohamed and co-workers [8, 35] showed that such approximate enrichment functions result in better accuracy and use less degrees of freedom, in comparison to conventional low-order polynomial based finite element solutions. In [8, 35], Gaussian functions are used to capture the time varying temperature fields. Similar enrichment functions for solving transient heat transfer problems are

also proposed in [36, 37].

The fact that enrichment-based methods use coarse mesh grids for solution approximation, the proper selection of enrichment functions is of vital importance for the good performance of these methods. The relative errors in the energy norm may rise to 40% or more in case of non-conforming enrichment functions [38]. To investigate the accuracy of approximate numerical methods, *a-posteriori* error estimation has become an important tool and has been used extensively by the research community. The current work presents the study of *a-posteriori* error estimate for the approximate solutions of transient conduction problems using GFEM. The basic motivation of the study is to provide an efficient and reliable tool for the selection of suitable enrichment functions with special emphasis on problems with unknown analytical solutions. In this work, we use two types of enrichment functions to enrich the approximation space and capture the sharp thermal gradients on coarse finite element meshes. The presented error estimate is utilized as a tool to assess the performance of the selected enrichment functions and help in selecting better alternative functions that produce lower errors. Problems in 2D and 3D domains are selected to show that the proposed error estimate does not depend on the scale of the problem and is equally applicable to 2D as well as 3D problems. Numerical results indicate that the proposed error estimate provides a reliable tool to select better enrichment functions for a given problem.

This paper is organised as follows. After the introduction, Section 2 presents the formulation of the heat conduction problem followed by its weak form and GFEM discretization. The formulation of the considered enrichment functions is also presented in Section 2. The residual *a-posteriori* error estimate is introduced in Section 3, with its algorithmic considerations in Section 4. The main numerical computations are presented in Section 5. Conclusions of the study are presented in Section 6.

2. Problem formulation

This section describes the formulation of the time-dependent conduction heat transfer problem followed by its weak formulation to be solved by GFEM approximation.

2.1. Boundary value problem

Consider a bounded open domain, $\Omega \subset \mathbb{R}^n, n = 2, 3$, bounded by Γ, and a time interval $]0, t_f]$. The governing equation of the considered transient conduction heat transfer problem is given by

$$\frac{\partial \phi}{\partial t} - \lambda \Delta \phi = G(t, \mathbf{x}), \qquad (t, \mathbf{x}) \in]0, t_f] \times \Omega \ , \tag{1}$$

where ϕ is the unknown temperature field whereas t and $\mathbf{x} = (x, y, z)^T$ are the time and spatial variables, respectively. The parameter λ denotes the heat diffusion coefficient and $G(t, \mathbf{x})$

represents the source term. We consider the following initial condition

$$\phi(t=0,\mathbf{x}) = \phi_0(\mathbf{x}), \qquad (\mathbf{x}) \in \Omega \ , \tag{2}$$

where $\phi_0(\mathbf{x})$ denotes a prescribed initial temperature field. A Robin type boundary condition is applied on the the outer boundary Γ. It is given by

$$\frac{\partial \phi}{\partial \mathbf{n}} + \alpha\phi = g(t,\mathbf{x}), \qquad (t,\mathbf{x}) \in]0,t_f] \times \Gamma \ , \tag{3}$$

where $\mathbf{n}$ is the outward unit normal on Γ, Δ is the Laplacian operator, α is the convection heat coefficient and $g(t,\mathbf{x})$ denotes a boundary source.

2.2. Weak formulation

To find the approximate solution of the boundary value problem given by (1)–(3), we first present the weak formulation using the Galerkin procedure. For the time discretization an implicit Euler scheme is used.

2.2.1. Galerkin procedure

We use the standard Galerkin procedure and multiply (1) with a weight function ω and integrate it over Ω.

$$\int_\Omega \left(\omega \frac{\partial \phi}{\partial t} - \omega\lambda\Delta\phi \right) d\Omega = \int_\Omega \omega G \ d\Omega \ . \tag{4}$$

To eliminate the second derivative term in the above equation, the Green's lemma is used which results in

$$\int_\Omega \left(\omega \frac{\partial \phi}{\partial t} + \lambda\nabla\omega\nabla\phi \right) d\Omega - \int_\Gamma \lambda\omega\nabla\phi\cdot n \ d\Gamma = \int_\Omega \omega G \ d\Omega \ , \tag{5}$$

The substitution of the boundary condition (3) in (5) results in the weak form of the transient conduction problem, whihc reads as follows: Find an approximate solution ϕ on domain Ω with the initial condition ϕ_0 and for all test functions ω on Ω and all $n \in \mathbb{N}$ such that

$$\int_\Omega \left(\omega \frac{\partial \phi}{\partial t} + \lambda\nabla\omega\nabla\phi \right) d\Omega + \int_\Gamma \lambda\omega\alpha\phi \ d\Gamma = \int_\Omega \omega G \ d\Omega + \int_\Gamma \lambda\omega g \ d\Gamma. \tag{6}$$

2.2.2. Time discretization

To discretize (6) in time we use an implicit Euler scheme. We divide the time $[0,t_f]$ into a number N_t of small intervals $[t_n,t_{n+1}]$ of size $\delta t = t_{n+1} - t_n$. The time derivative in the weak form (6) is approximated by a difference quotient. The problem (6) becomes

$$\int_\Omega \left(\omega \frac{\phi^{n+1}-\phi^n}{\delta t} + \lambda\nabla\omega\nabla\phi^{n+1} \right) d\Omega + \int_\Gamma \lambda\omega\alpha\phi^{n+1} d\Gamma = \int_\Omega \omega G^{n+1} d\Omega + \int_\Gamma \lambda\omega g^{n+1} d\Gamma, \tag{7}$$

where ϕ^{n+1} and ϕ^n are the temperature field solutions at times t_{n+1} and t_n, respectively. Rearranging results in the time–discretized variant of the weak formulation (6): Find a solution ϕ^{n+1} on Ω such that $\phi^0 = \phi_0$ and for all test functions ω on Ω and all $n \in \mathbb{N}$ such that

$$\int_\Omega (\nabla\omega\cdot\nabla\phi^{n+1} + \omega\beta \ \phi^{n+1}) d\Omega + \int_\Gamma \omega\alpha \ \phi^{n+1} d\Gamma = \int_\Omega \omega P^{n+1} d\Omega + \int_\Gamma \omega g^{n+1} d\Gamma \ , \tag{8}$$

where P^{n+1} and β are defined by

$$P^{n+1} = \beta\Big(\delta t G(t_{n+1}, \mathbf{x}) + \phi^n\Big) \ , \qquad \beta = \frac{1}{\lambda \delta t} \ .$$

Our aim is to find an approximate numerical solution ϕ^{n+1} of the weak formulation (8) using the GFEM formulation.

2.3. GFEM discretization

To find an approximate numerical solution of the weak formulation (8) with the GFEM formulation, the domain Ω is discretized into a number n_e of non-overlapping elements Ω_e such that $\Omega = \cup\Omega_e$. The solution in each element is then approximated by a combination of piecewise linear shape functions and enrichment functions and so we look for $\phi^{n+1}(\mathbf{x})$ of the form

$$\phi^{n+1}(\mathbf{x}) = \sum_{j=1}^{M}\sum_{q=1}^{Q} N_j(\mathbf{x}) A_j^q \Psi(\mathbf{x}). \tag{9}$$

Here $N_j(\mathbf{x})$ are the Lagrange shape functions and M is the number of nodes in the element. $\Psi(\mathbf{x})$ are the GFEM enrichment functions with A_j^q being their coefficients at the nodal points and Q denotes the number of enrichment functions. For ease of notation, we take $N_j(\mathbf{x})\Psi(\mathbf{x}) = \Re_n$. In (9) the standard polynomial shape functions $N_j(\mathbf{x})$ with $j = 1, ...M$, constitutes the partition of unity, i.e. $\sum_{j=1}^{M} N_j(\mathbf{x}) = 1$. It is worth mentioning that the current formulation, unlike the discontinuous enrichment method or the ultraweak variational formulation, is continuous thanks to the use of the polynomial shape functions N_j.

The literature reveals instances where enrichment functions are applied locally [39–41], but for the current GFEM formulation, we use multiple enrichment functions of global nature. In order to show the working of the proposed error estimate, defined in the next section, and to carry out a comparative study of enrichment functions, two different types of enrichment functions are considered in this current study. In the first type, the enrichment functions are based on *Gaussian* functions as used in [8, 42], while the second type of enrichment is based on *sin* functions and is a variation of the functions used in [43] for one-dimensional diffusion-convection problems. The formulation of both enrichment functions is given below.

Type EF1: Gaussian enrichment functions

$$\Psi 1(\mathbf{x}) = \frac{e^{-\left(\frac{R_0}{C}\right)^q} - e^{-\left(\frac{R_c}{C}\right)^q}}{1 - e^{-\left(\frac{R_c}{C}\right)^q}} \ , \qquad q = 1, 2, \ldots, Q \tag{10}$$

Type EF2: *sin* enrichment functions

$$\Psi 2(\mathbf{x}) = 1 - \left(sin^4\left(\frac{R_0}{L_0}\right)\right)^{A_0 q}, \qquad q = 1, 2, \ldots, Q \tag{11}$$

In the above equations, the parameters R_c and C, in EF1, and A_0 and L_0, in EF2, are constants which control the shape of $\Psi(\mathbf{x})$, while R_0 is the distance of any point $\mathbf{x}$ in the domain from a fixed

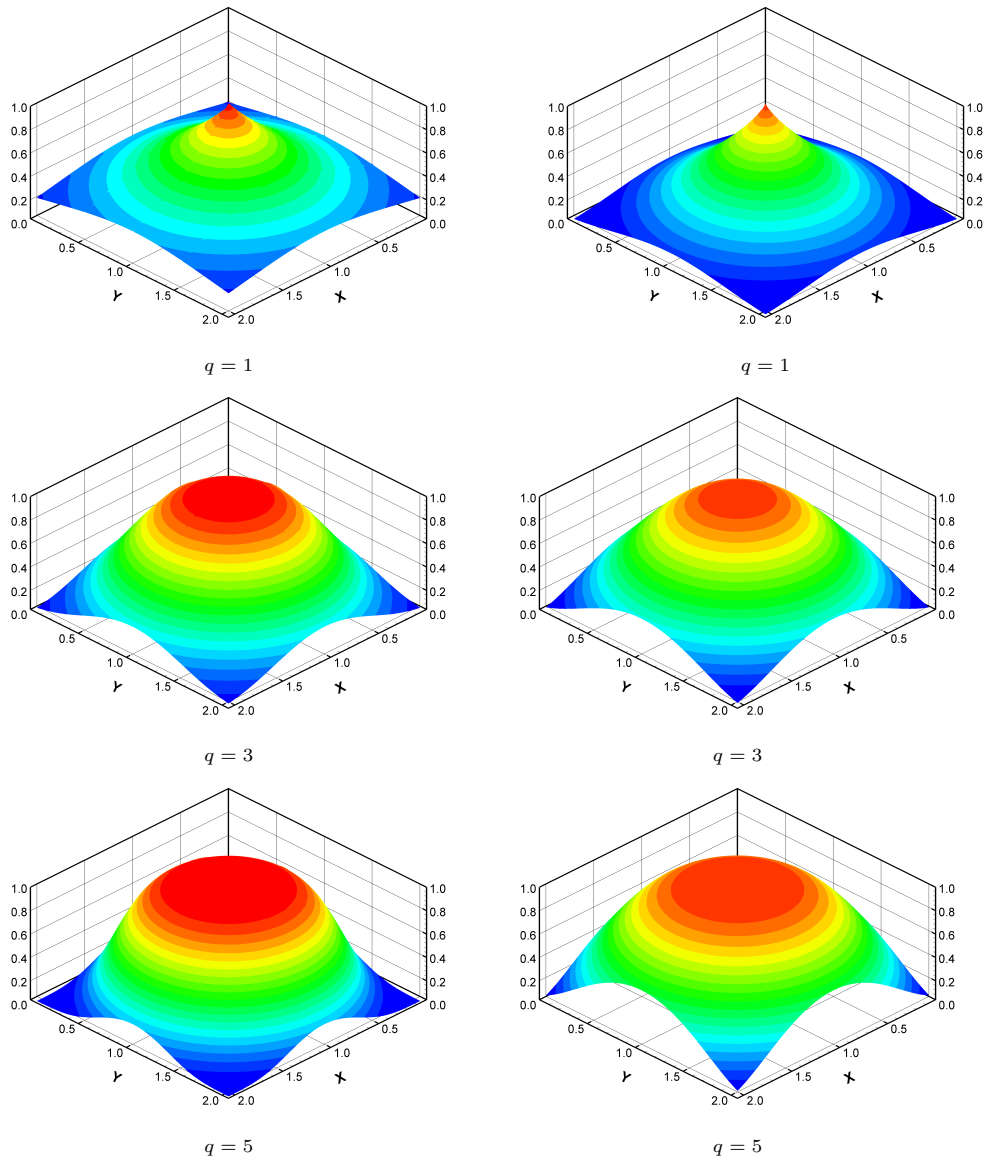

Figure 1: Illustration of EF1 (left column) and EF2 (right column), for different values of q.

point $\mathbf{x}_c$, which is defined as $R_0 := |\mathbf{x} - \mathbf{x}_c|$. In general, the fixed point $\mathbf{x}_c$ represents the centre of the enrichment functions. The steepness of the enrichment functions given by both types EF1 and EF2 is controlled by the parameter q such that smaller values of q result in rapidly varying enrichment functions which are useful in capturing solutions with sharp thermal gradients. On the other hand, higher values of q produce slowly varying enrichment functions which can be useful when the temperatures become more uniform. Figure 1 illustrates the variation of EF1 and EF2 types enrichment functions for different values of q.

In the standard Galerkin procedure, the weighting functions ω are taken to be the same as the shape functions N_j. For GFEM we take $\omega = \Re_n$ which results in the GFEM discretization of

the weak form (8) such that:

Find $\phi^{n+1}(\mathbf{x})$ of the form (9) such that initial temperature $\phi^0 = \phi_0$ and for all $n = 1, ..., MQ$

$$\int_\Omega (\nabla \Re_n \cdot \nabla \phi^{n+1} + \Re_n \beta \phi^{n+1}) d\Omega + \int_\Gamma \Re_n \alpha \phi^{n+1} d\Gamma = \int_\Omega \Re_n P^{n+1} d\Omega + \int_\Gamma \Re_n g^{n+1} d\Gamma \ . \quad (12)$$

The enrichment functions Ψ are formulated in the global co-ordinates and modulated locally by multiplying them with local shape functions N_j. The choice of the enrichment functions is driven by the physical behaviour of the solution. In general, little can be known about their approximation properties. However, enhanced enrichment functions can be chosen for a specific problem by accurately assessing the discretization error, which is the main motivation for presenting this current study.

3. A residual *a-posteriori* error estimate

From the approximate numerical solution ϕ^{n+1} at time t_{n+1}, we define the solution $\phi(t, \mathbf{x})$ for all positive t

$$\phi(t, \mathbf{x}) = \frac{t - t_n}{t_{n+1} - t_n} \ \phi^{n+1}(\mathbf{x}) + \frac{t_{n+1} - t}{t_{n+1} - t_n} \ \phi^n(\mathbf{x}) \ ,$$

for all $t \in]t_n, t_{n+1}]$ and the definitions of $\hat{\phi}(t, \mathbf{x})$, $\hat{G}(t, \mathbf{x})$ and $\hat{g}(t, \mathbf{x})$

$$\begin{aligned} \hat{\phi}(t, \mathbf{x}) =& \phi(t_{n+1}, \mathbf{x}) \ , \\ \hat{G}(t, \mathbf{x}) =& G(t_{n+1}, \mathbf{x}) \ , \\ \hat{g}(t, \mathbf{x}) =& g(t_{n+1}, \mathbf{x}) \ , \end{aligned}$$

the time discretized version (7) can be written as

$$\int_\Omega \left(\Re_n \partial_t \phi + \lambda \nabla \Re_n \nabla \hat{\phi} \right) d\Omega + \int_\Gamma \lambda \Re_n \alpha \hat{\phi} \ d\Gamma = \int_\Omega \Re_n \hat{G} \ d\Omega + \int_\Gamma \lambda \Re_n \hat{g} \ d\Gamma \ . \quad (13)$$

In the above notation, a classical residual based *a-posteriori* error estimate, similar to the widely used estimates for adaptive $h-$FEM and $hp-$FEM, is obtained for the GFEM solution. In the current work, we aim to find the accuracy of the two types of chosen enrichment functions with the help of the error estimation procedure.

As per *Theorem 1* of [42], if Φ is the exact solution of the weak form (6) and ϕ denotes the approximate solution of the GFEM discretization (12), then there exists a constant $c > 0$ such that

$$\begin{aligned} \int_\Omega |\Phi(t, \mathbf{x}) - \phi(t, \mathbf{x})|^2 d\Omega + \lambda \int_0^{t_f} \int_\Omega |\nabla(\Phi - \hat{\phi})|^2 d\Omega \ dt \\ \leq c\{\eta_1^2 + \eta_2^2 + \eta_3^2 + \eta_4^2 + \eta_5^2 + \eta_6^2\}. \end{aligned} \quad (14)$$

The terms on the left hand side (LHS) of (14) present the actual errors incurred in the solution obtained by the GFEM approximation, while the terms on the right hand side (RHS) present the computable error indicators $\eta_1^2, \eta_2^2, ...\eta_6^2$, which are defined as follows.

$$\eta_1^2 = \|\Phi_0 - \phi_0\|^2_{L^2(\Omega)}, \tag{15}$$

$$\eta_2^2 = \sum_K \int_0^{t_f} \left\| \hat{G} - \partial_t \phi + \lambda \Delta \hat{\phi} \right\|^2_{H^{-1}(K)} dt, \tag{16}$$

$$\eta_3^2 = \int_0^{t_f} \left\| G - \hat{G} \right\|^2_{H^{-1}(\Omega)} dt + \lambda \int_0^{t_f} \|\hat{g} - g\|^2_{H^{-1/2}(\Gamma)} \; dt, \tag{17}$$

$$\eta_4^2 = \lambda \int_0^{t_f} \left\| \nabla(\phi - \hat{\phi}) \right\|^2_{L^2(\Omega)} dt, \tag{18}$$

$$\eta_5^2 = \sum_{E \cap \Gamma = \emptyset} \int_0^{t_f} \left\| \left[\frac{\partial \hat{\phi}}{\partial n} \right] \right\|^2_{L^2(E)} dt, \tag{19}$$

$$\eta_6^2 = \lambda \int_0^{t_f} \left\| \hat{g} - \frac{\partial \hat{\phi}}{\partial n} - \alpha \hat{\phi} \right\|^2_{H^{-1/2}(\Gamma)} dt. \tag{20}$$

In order to test the accuracy of GFEM for transient heat conduction problems, both LHS and RHS need to be computed. For an acceptable accuracy, RHS will always bound LHS. In [42], the error indicators were derived and were shown to accurately capture the error of the numerical solution. Here, we use the indicators as a tool to assess the accuracy of the numerical approximation by two types of enrichment functions. As we are concerned with the application of the error estimate therefore only RHS is calculated to assess the accuracy of EF1 and EF2 enrichment functions. The defined error indicators have clear physical meanings. The first one, η_1, measures the error introduced by the approximation of the initial condition (2) and η_6 measures the violation of the boundary condition (3). The violation of the original governing equation (1) is measured by η_2 while the error in the approximation of the source term is described by η_3. The errors involved in the time discretization are calculated by η_4 and, last, η_5 measures the jump of the numerical solution across the boundaries of adjoining elements. The error indicators estimate the approximation error of the finite element solution independently of the choice of the enrichment functions. This was the main motivation in their derivation in [42]. From the definition of the error indicators (15)–(20), it is clear that they are independent of the heuristically selected enrichment functions and can be used for any kind of enrichment. While in the current study the indicators are used to estimate the errors for EF1 and EF2, they are equally applicable for other choices of enrichment functions. For further details and proof of *Theorem 1*, readers are referred to [42].

4. Implementation of the algorithm

The computation procedure of the error indicators $\eta_1^2, \eta_2^2, ...\eta_6^2$ is described in this section. In the numerical computations, only indicators $\eta_2^2,\ \eta_4^2$ and η_5^2 are calculated, while $\eta_1^2,\ \eta_3^2$ and η_6^2 are neglected. The indicator η_1^2, which measures the error in the approximation of the initial condition, vanishes for the initial condition $\phi_0 = 0$ considered here. The exact implementation of source term G and boundary source g sets the indicator $\eta_3^2 = 0$. Similarly, the indicator η_6^2 is ignored due to its negligibly small value. The indicators $\eta_2^2,\ \eta_4^2$ and η_5^2 are computed individually in the whole domain. However, an overall value of the error estimate η is presented in the discussion of the numerical results. It is defined by

$$\eta = \left(\eta_2^2 + \eta_4^2 + \eta_5^2\right)^{1/2}. \tag{21}$$

The procedure for calculation of $\eta_2,\ \eta_4$ and η_5 relies on certain numerical approximations rather than calculating the indicators exactly. For example, the indicator η_2^2 is approximated as

$$\eta_2^2 = \sum_{n=0}^{N_t} \sum_K \eta_2^2(n, K), \tag{22}$$

with

$$\begin{aligned}
\eta_2^2(n,K) &= \int_{t_n}^{t_{n+1}} \left\| \hat{G} - \partial_t \phi + \lambda \Delta \hat{\phi} \right\|^2_{H^{-1}(K)} \\
&\leq \int_{t_n}^{t_{n+1}} dt \int_K \left(\hat{G} - \partial_t \phi + \lambda \Delta \hat{\phi} \right)^2 d\Omega \\
&= \frac{\delta t}{2} \int_K \left(G^{n+1} - \frac{\phi^{n+1} - \phi^n}{\delta t} + \lambda \left(\frac{\partial^2 \phi^{n+1}}{\partial x^2} + \frac{\partial^2 \phi^{n+1}}{\partial y^2} + \frac{\partial^2 \phi^{n+1}}{\partial z^2} \right) \right)^2 d\Omega \\
&+ \frac{\delta t}{2} \int_K \left(G^{n} - \frac{\phi^{n+1} - \phi^n}{\delta t} + \lambda \left(\frac{\partial^2 \phi^{n}}{\partial x^2} + \frac{\partial^2 \phi^{n}}{\partial y^2} + \frac{\partial^2 \phi^{n}}{\partial z^2} \right) \right)^2 d\Omega.
\end{aligned}$$

For accurate computations, the values of G and ϕ are calculated at present as well as at previous time steps. All the values are calculated at each integration point and then the accumulated value is determined for the whole domain.

The indicator η_4^2 is approximated as

$$\eta_4^2 = \sum_{n=0}^{N_t} \sum_K \eta_4^2(n, K), \tag{23}$$

with

$$\begin{aligned}
\eta_4^2(n,K) &= \lambda \int_{t_n}^{t_{n+1}} \left\| \nabla(\phi - \hat{\phi}) \right\|^2_{L^2(K)} \\
&= \lambda \int_{t_n}^{t_{n+1}} \left(\frac{t_{n+1} - t}{t_{n+1} - t_n} \right)^2 dt \int_K \left[\left(\frac{\partial \phi^{n+1}}{\partial x} - \frac{\partial \phi^n}{\partial x} \right)^2 + \left(\frac{\partial \phi^{n+1}}{\partial y} - \frac{\partial \phi^n}{\partial y} \right)^2 + \left(\frac{\partial \phi^{n+1}}{\partial z} - \frac{\partial \phi^n}{\partial z} \right)^2 \right] d\Omega \\
&= \frac{\lambda \delta T}{3} \left(\int_K \left(\frac{\partial \phi^{n+1}}{\partial x} - \frac{\partial \phi^n}{\partial x} \right)^2 d\Omega + \int_K \left(\frac{\partial \phi^{n+1}}{\partial y} - \frac{\partial \phi^n}{\partial y} \right)^2 d\Omega \right. \\
&\left. + \int_K \left(\frac{\partial \phi^{n+1}}{\partial z} - \frac{\partial \phi^n}{\partial z} \right)^2 d\Omega \right) .
\end{aligned}$$

Here the definition of $\phi(t,\mathbf{x}) - \hat{\phi}(t,\mathbf{x})$ is used as

$$\phi(t,\mathbf{x}) - \hat{\phi}(t,\mathbf{x}) = -\frac{t_{n+1}-t}{t_{n+1}-t_n}\left(\phi^{n+1}(\mathbf{x}) - \phi^{n}(\mathbf{x})\right).$$

In the expression of the indicator η_4^2, the derivatives of ϕ with respect to the spatial coordinates are calculated at each integration point and then accumulated for the whole computational domain.

The indicator η_5^2 is approximated as

$$\eta_5^2 = \sum_{n=0}^{N_t}\sum_{E}\eta_5^2(n,E)$$

with

$$\begin{aligned}
\eta_5^2(n,E) &= \int_{t_n}^{t_{n+1}} \left\| \left[\frac{\partial\hat{\phi}}{\partial n}\right] \right\|^2_{L^2(E)} dt \\
&= \int_{t_n}^{t_{n+1}} \left\| \left[\nabla\phi^{n+1}\cdot\mathbf{n}\right] \right\|^2_{L^2(E)} dt \\
&= \int_{t_n}^{t_{n+1}} \int_E \left(\nabla\phi_{E_1}^{n+1} n_1 + \nabla\phi_{E_2}^{n+1} n_2\right)^2 dE\, dt \\
&= \int_{t_n}^{t_{n+1}} \int_E \left(\nabla\phi_{E_1}^{n+1} n_1 - \nabla\phi_{E_2}^{n+1} n_1\right)^2 dE\, dt \\
&= \delta t \int_E \Bigg(\left(\frac{\partial\phi^{n+1}}{\partial x} n_{1_x} + \frac{\partial\phi^{n+1}}{\partial y} n_{1_y} + \frac{\partial\phi^{n+1}}{\partial z} n_{1_z}\right)_{E_1} \\
&\quad - \left(\frac{\partial\phi^{n+1}}{\partial x} n_{1_x} + \frac{\partial\phi^{n+1}}{\partial y} n_{1_y} + \frac{\partial\phi^{n+1}}{\partial z} n_{1_z}\right)_{E_2} \Bigg)^2 dE\,.
\end{aligned}$$

Here, E_1 and E_2 represent the edges of two adjacent elements while $n_1 = -n_2$ are their unit normals, respectively. It is worth mentioning that the formulations of η_2^2, η_4^2 and η_5^2 are presented above for 3D spatial domains. For 2D domains, the derivatives terms with respect to z are simply eliminated. While originally derived for 2D heat diffusion problems, the formulation of the error indicators is not restricted to 2D domains and is equally applicable for problems in 3D domains. In a recent contribution [44], their formulation is validated for 3D problems. The current work is concerned with the application of the error indicators for the selection of better performance enrichment functions for problems in 2D as well as in 3D domains.

5. Numerical tests and results

This section presents numerical results showing the effectiveness of the presented *a-posteriori* error estimate to measure the accuracy of GFEM solutions of transient heat conduction problems using two different types of enrichment functions. The proposed error estimate is shown to be used as a tool to test the performance of the selected enrichment functions and help in selecting

enrichment functions with better accuracy. To show the effectiveness of the error estimate, problems in 2D and 3D domains are considered. The first example considers a problem in 2D domain with a known analytical solution. The second and third example problems aim to show the usefulness of the proposed error estimate for more general cases where the exact solutions are not known. The numerical computations for 2D problems are carried out with 4-noded quadrilateral elements whereas 3D computations are performed with 8-node hexahedral elements. All integrations are performed numerically using Gauss–Legendre quadrature procedure. In order to avoid the errors from the integration procedure, a preliminary study was performed and based on the results obtained with 20 integration points in each spatial direction are used for all the computations presented in this study. All the physical quantities used in the numerical experiments are measured in a consistent system of units. For simplicity, all the quantities are mentioned without units. This is emphasized by the purpose of this study to establish that the developed error estimate can be used as a tool to test the performance of enrichment functions. If a range of enrichment functions are proposed for a specific problem or a class of problems, the developed error estimate can help in the selection of most effective enrichment functions. It can also be used to enhance the shape of an enrichment function to reduce the overall discretization errors.

5.1. Example problem 1

The first considered example presents the application of the developed error estimate for a problem with known analytical solution. For a square domain $\Omega = [0, 2]^2$, we take $u_0(\mathbf{x})$, $G(t, \mathbf{x})$ and $g(t, \mathbf{x})$ such that the exact solution of (1)-(3) is given by

$$\Phi_{ext}(\mathbf{x}, t) = x^\tau (2 - x)^\tau y^\tau (2 - y)^\tau (1 - e^{-\lambda t}). \tag{24}$$

For numerical computations, we select $\tau = 20$ to produce steep temperature gradients. For a problem with known analytical solution Φ_{ext}, the relative L_2 norm error (ε) can be calculated by

$$\varepsilon\% \ = \frac{||\Phi_{ext} - \phi||_{L^2(\Omega)}}{||\Phi_{ext}||_{L^2(\Omega)}} \times 100. \tag{25}$$

The intention behind the selection of a problem with known analytical solution is to show that the proposed error estimate behaves in the same manner as the L_2-norm error defined above. In the computations, the values of η and $\varepsilon\%$ are calculated for both types of the enrichment functions. In the presented results it is established that both η and $\varepsilon\%$ behave alike when the number of enrichment functions is varied or the mesh size is changed. The effect of the condition number (κ) on η and $\varepsilon\%$ is also investigated with $q-$ and $h-$refinements. The results provide basis for establishing the fact that the proposed error estimate can be effectively used as a tool to test the accuracy of the results for problems with no available analytical solutions.

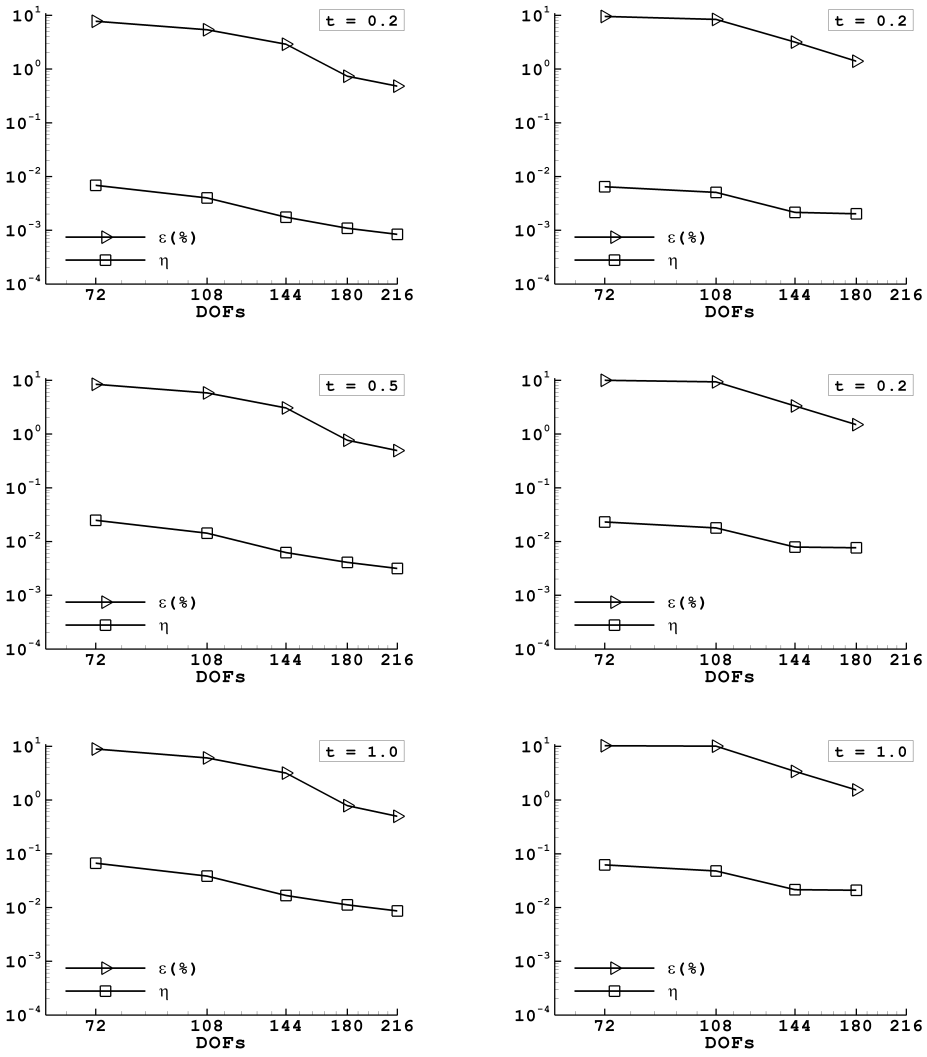

Figure 2: Variation of $\varepsilon\%$ and η with $q-$refinement for EF1 (left column) and EF2 (right column).

For numerical computations, the parameters α and λ are taken to be 1 and 0.1, respectively. The time step value is set to be $\delta t = 0.01$ with a total solution time of $t = 1.0$. The effects of $q-$refinement, $h-$refinement and condition number κ are analysed for both types of enrichment functions and based on the results, enrichment functions with better performance are identified.

5.1.1. Effect of $q-$refinement

As a first study, we evaluate the effect of the number of enrichment functions on the error estimate and L_2 norm error. For a fixed coarse mesh of 125 elements, we increase the number of enrichment functions, $Q = 2, 3, \ldots 6$, and compute η and $\varepsilon\%$ for EF1 and EF2. The total number of degrees of freedom (DOFs) for each number of enrichment functions is given in Table 1.

Table 1: Total DOFs corresponding to each number of enrichment functions Q.

Case	Q	DOFs
1	2	72
2	3	108
3	4	144
4	5	180
5	6	216

Figure 2 shows the variation of the error estimate η and the L_2-norm error $\varepsilon\%$ for both versions of enrichment functions with increasing Q at three different simulation times, $t = 0.2$, 0.5 and 1.0. In the figure, the total number of degrees of freedom DOFs as given in Table 1 is presented on the abscissa while the error estimate η along with the relative L_2-norm error $\varepsilon\%$ are shown on the ordinate. The values of η and $\varepsilon\%$ are of different orders and so the logarithmic scale is used for plotting the variation of the two quantities. The results show that in all cases, the errors decrease with the increase of Q and hence DOFs. Both η and $\varepsilon\%$ show similar decreasing trend. Comparison of the results show that relatively lower errors are obtained using EF1 with the minimum error obtained with $Q = 6$ (216 DOFs). For EF2, the errors decrease with increasing Q up to $Q = 5$ (180 DOFs) and then further increase of Q does not improve the results. In fact, the results corresponding to $Q = 6$ are not shown because of the induced increase of both the error estimate η along with the relative L_2-norm error $\varepsilon\%$. The deterioration of the results with higher Q is attributed to the very high condition number of the system matrix due to the enrichment functions EF2. This is presented and discussed in the subsequent sections.
Figure 3 depicts the temperature distribution obtained with the exact solution and GFEM, with EF1 and EF2. It is clear that GFEM solutions show temperature profiles similar to the exact solution. An important observation made from Figure 3 is although very similar temperature profiles are obtained with EF1 and EF2, yet the performance of EF1 is better than EF2, as concluded from Figure 2. This shows the usefulness of the proposed error estimate, which provides errors in the solution, the derivatives of the solution as well as in the initial condition, boundary condition and source term, and therefore offers a reliable tool to thoroughly test the accuracy of numerical solutions of transient conduction problems.

5.1.2. Effect of h−refinement

The second study tests the performance of the EF1 and EF2 types of enrichment functions with the mesh size h of the computational domain. For this study, we fix the number of enrichment functions $Q = 5$ and change the mesh size. We start with a mesh of 4×4 elements and enrich the solution space with 5 enrichment functions. Three other mesh grids are considered with 5×5

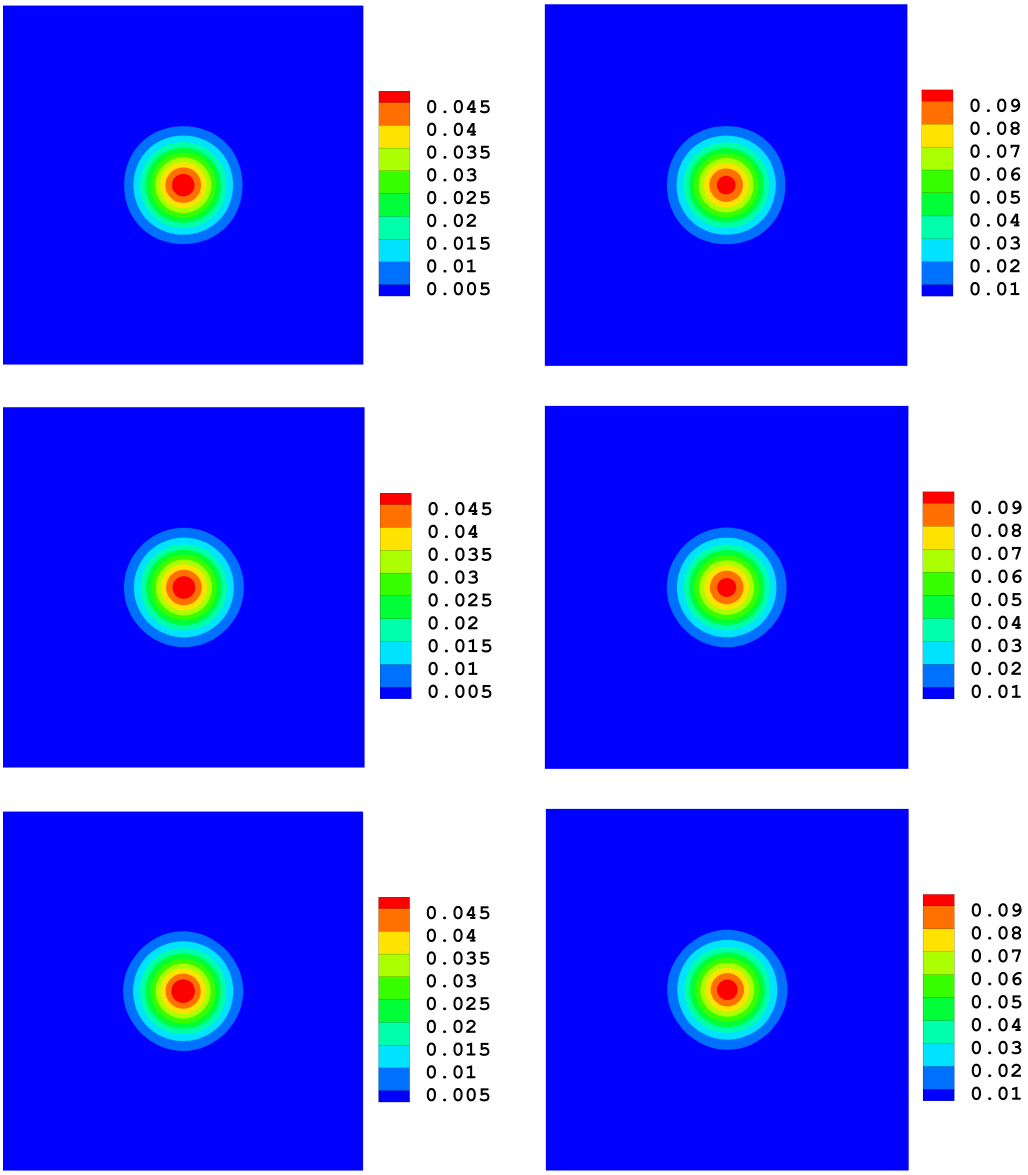

Figure 3: Temperature profiles obtained with the exact solution (top row) and GFEM solution with EF1 (centre row) and with EF2 (bottom row) at times $t = 0.5$ (left column) and $t = 1.0$ (right column).

, 6×6 and 8×8 elements. The total number DOFs for the selected four mesh grids are 125, 180, 245 and 405, respectively.

To compare the results of the EF1 and EF2 types of enrichment functions, the error estimate η and the relative L_2-norm error are evaluated and plotted against the total number of degrees of freedom. Figure 4 shows the results at three selected simulation times. As in the previous study, comparatively lower errors are obtained with EF1 at all computation times. From the results, it is clear that the error estimate η and relative L_2-norm error $\varepsilon\%$ show similar behaviour as both decrease with the increase in the mesh density. A sustained decrease is observed for the case of

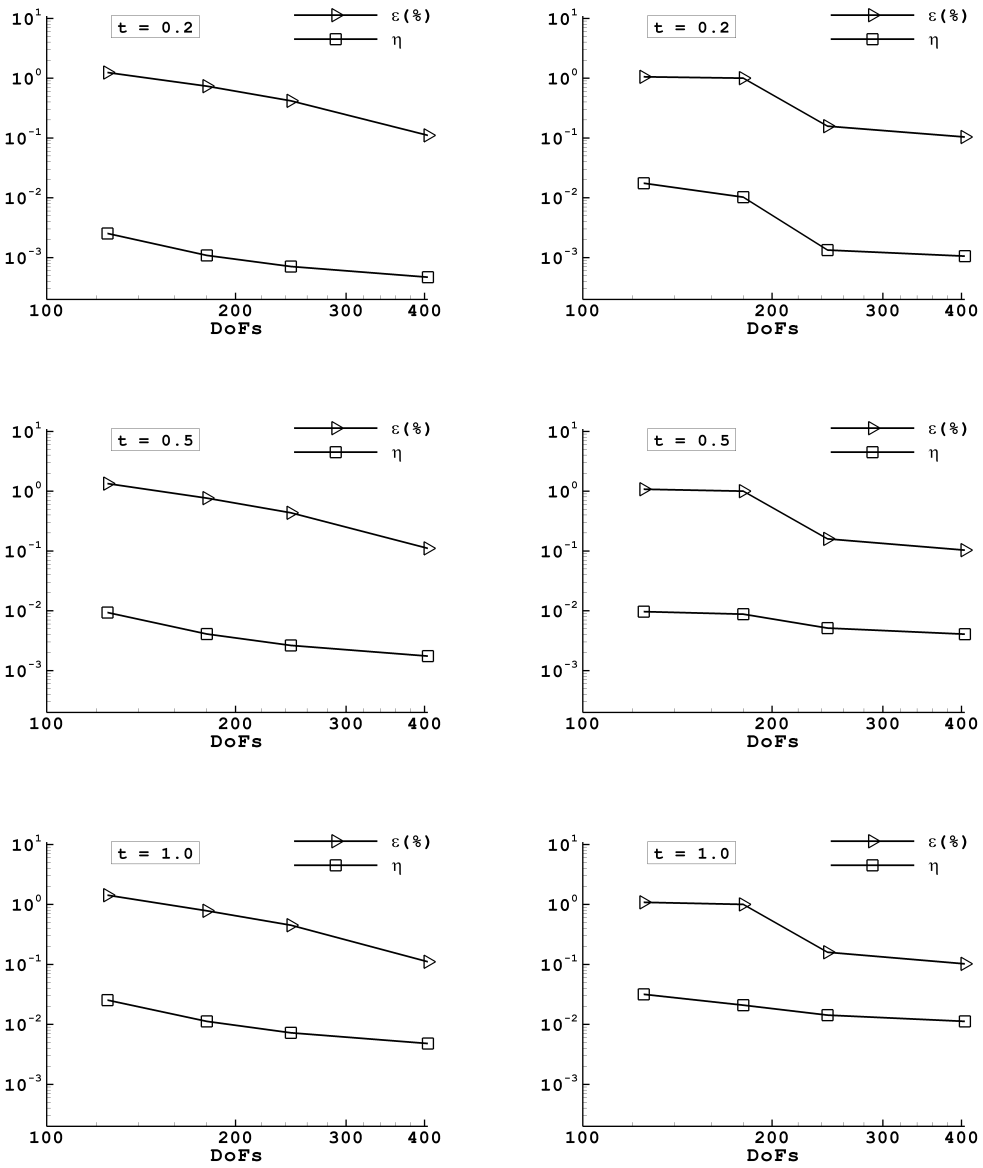

Figure 4: Variation of $\varepsilon\%$ and η with $h-$refinement for EF1 (left column) and EF2 (right column).

EF1 while, in the case of EF2, improvement in the results by increasing mesh density from 4×4 to 5×5 is small. A rapid decrease is noticed with 6×6 mesh and a further small improvement in the errors with 8×8 mesh. The comparison of the results of both enrichment functions shows EF1 to perform better than EF2, for the considered problem.

Table 2: Variation of Condition Number (κ) with increasing Q for EF1 and EF2.

Q	κ(EF1)	κ(EF2)
3	8.64E+07	6.42E+08
4	1.66E+11	8.16E+12
5	2.19E+13	3.50E+15
6	8.29E+15	8.68E+16
7	1.91E+17	2.00E+17

5.1.3. Effect of the Condition Number (κ)

Lins et al. [45] mentioned the ill-conditioning of system matrix as an inherent drawback of the GFEM formulation when a large number of enrichment functions is used. Different methodologies, including Stable GFEM [11], are proposed to improve the conditioning issue of GFEM. This study is designed to show the effect of the condition number κ on the results deterioration when a large number of enrichment functions or a fine mesh grids are used. The purpose here is not to improve the conditioning issue of the GFEM method, but to show that the proposed error estimate efficiently captures the effect of ill-conditioning on the GFEM results.

To study the effect of the condition number on the results quality obtained with EF1 and EF2 types of enrichment functions, a uniform mesh of 8×8 elements is selected with $Q = 3, 4, ...7$ to perform the numerical computations. The variation of η and $\varepsilon\%$ with increasing Q is depicted in Figure 5 for both enrichment functions. For EF1, the values of η and $\varepsilon\%$ decrease up to $Q = 6$ and a further increase in the number of enrichment functions leads to an ill-conditioned system and the deterioration of the solution, as commonly encountered in GFEM. For EF2, the decrease of η and $\varepsilon\%$ is observed up to $Q = 5$ and then with $Q = 6$ the results deteriorate which can be clearly seen in Figure 5(b). The results become then irrelevant for $Q = 7$ as the values of η and $\varepsilon\%$ increase significantly. Table 2 shows the values of the condition number for EF1 and

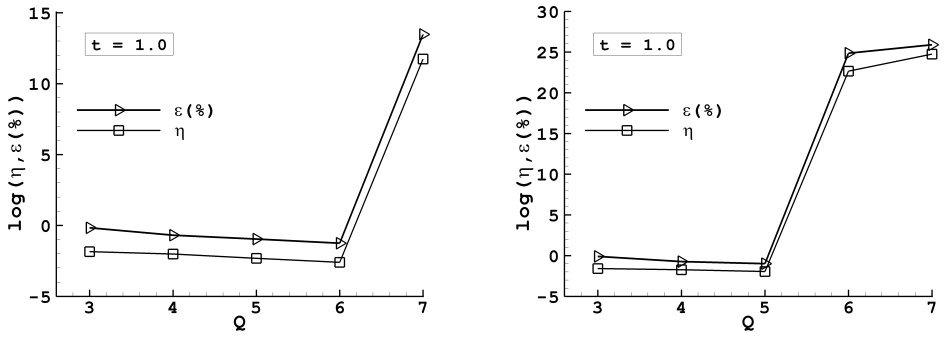

(a) EF1 (b) EF2

Figure 5: Result deterioration of $\varepsilon\%$ and η with higher Q.

EF2 enrichment functions for increasing values of Q. It is clear that the GFEM formulation with EF1 results in relatively lower condition numbers in comparison to the numbers corresponding to EF2. With $Q = 3$, relatively low values of κ are obtained for both types of enrichment functions. Increasing the number of enrichment functions leads to significant increase of the condition number for both EF1 and EF2 enrichment functions, with the EF2 related condition being at least one order of magnitude larger, in general. All the computations in this paper are performed using double-precision floating-point format. Hence, a condition number of around 1E+16 is expected to be a threshold where the resulting linear system of equations becomes practically singular and one may expect a large numerical error. For $Q = 6$ the condition number for EF2 grows to a value of 8.68E+16 which leads the results obtained with EF2 to deteriorate. For EF1 we get a condition number of 8.29E+15 which still produces meaningful results. With $Q = 7$, both EF1 and EF2 result in almost identical condition numbers, of the order 1E+17. This leads to the deterioration of the results obtained with both types of enrichment functions. An overall conclusion drawn from the above three studies is that for the presented numerical problem, EF1 performs comparatively better than EF2. Although small differences in the results are observed for both types of enrichment functions, the proposed error estimate efficiently captures these small variations under the specified parameters.

5.1.4. Selection of enrichment functions

In the preceding studies, the presented formulation was used to test and compare the performance of two types of enrichment functions and it was concluded that EF1 performs better that EF2, for the considered problems. The current section explores the possible use of the proposed error estimate to further improve the results of EF1 enrichment functions by enhancing the enrichment functions. As stated earlier, the constants C and R_c in (10) control the shape of the enrichment functions. Here we use different combinations of the parameters C and R_c as shown in Table 3 to get the optimum shape of EF1 enrichment functions that provide the best approximate solution of the considered problem. The procedure for optimizing the shape of the enrichment functions can be described as: Given the enrichment function (10), find C and R_c such that the solution to the considered problem is best approximated. Mathematically we can write

$$\text{For (10), find } C \text{ and } R_c \text{ such that } \eta \rightarrow \min \tag{26}$$

A similar study for improving the shape of enrichment functions is also performed in [44]. In [46], Waisman and Belytschko proposed an optimization algorithm to find an unknown parameter for enhancing the shape of the enrichment functions for boundary layer problems. Although in [46] the authors devised an automatic procedure for parameter optimization, in the current work we manually select different combinations of parameters C and R_C. A procedure for the identification

Table 3: Different combinations of contacts C and R_c used EF1 enrichment functions.

CASE	C	R_c
1	$\sqrt{0.5}$	$\sqrt{6}$
2	$\sqrt{0.5}$	$\sqrt{8}$
3	$\sqrt{0.5}$	$\sqrt{10}$
4	$\sqrt{1}$	$\sqrt{6}$
5	$\sqrt{1}$	$\sqrt{8}$
6	$\sqrt{1}$	$\sqrt{10}$
7	$\sqrt{1.5}$	$\sqrt{6}$
8	$\sqrt{1.5}$	$\sqrt{8}$
9	$\sqrt{1.5}$	$\sqrt{10}$

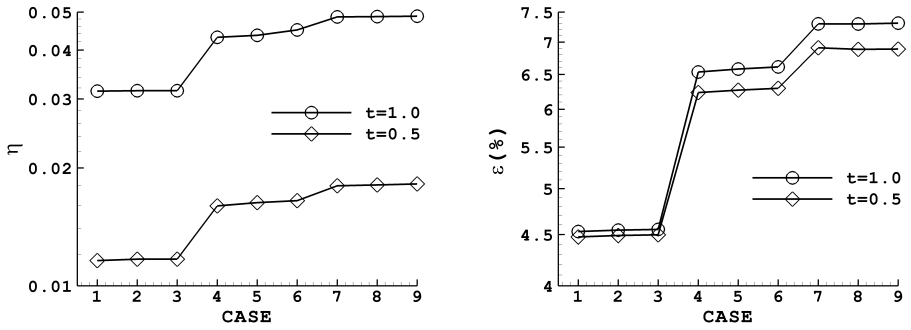

Figure 6: Variation of η and $\varepsilon\%$ with different combinations of C and R_c in EF1 enrichment functions.

of optimal local approximation spaces for GFEM solutions of elliptic partial differential equations is also formulated by Babuska and Lipton [47]. Figure 6 depicts the results of η along with $\varepsilon\%$ at two stated simulation times. It is clear from the figure that both η and $\varepsilon\%$ result in similar solution trends for different combinations of C and R_c. For problems with known analytical solutions, the L_2-norm error can be used as an indicator to select the best possible combination of C and R_c. However, for problems with no known analytical solutions where the L_2-norm error cannot be computed, the proposed error estimate can be used as a reliable tool to optimize the shape of the enrichment functions for minimal error.

Figure 6 shows that for the selected nine cases, CASE-1 with $C = \sqrt{0.5}$ and $R_c = \sqrt{6}$ produces the lowest errors while CASE-9 with $C = \sqrt{1.5}$ and $R_c = \sqrt{10}$ leads to the largest errors. It can also be observed from Figure 6 that the performance of the enrichment functions is predominantly dependent on the value of C and its variation with change in the values of R_c is small. For CASE-1 to CASE-3, where the value of C is constant and that of R_c is changing, we get almost constant values of η and L_2-norm error. For CASE-4, where the value of C changes from $\sqrt{0.5}$ to $\sqrt{1}$, we

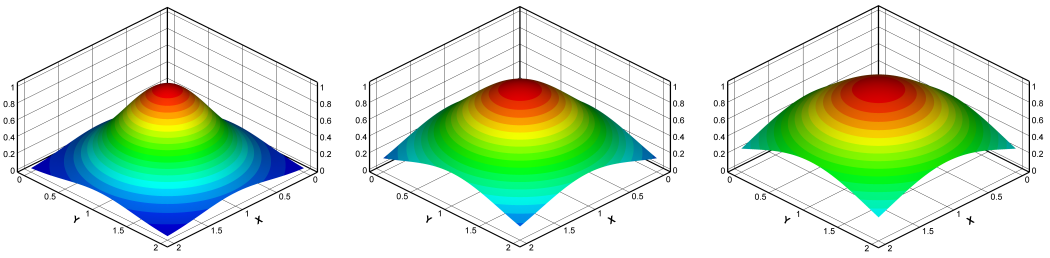

(a) CASE-1 (b) CASE-4 (c) CASE-7

Figure 7: Illustration of EF1 shape function with $q = 2$ for different combinations of C and R_c.

see a significant jump in the errors. Similarly, for CASE-7, where the value of C again changes from $\sqrt{1}$ to $\sqrt{1.5}$, an increase in the values of η and L_2-norm error can be observed. Figure 7 depicts how the shape of the enrichment functions changes with different combinations of C and R_c. Three cases; CASE-1, CASE-4 and CASE-7 are selected for illustration where a clear variation in the shape of the enrichment functions can be observed. It can be seen that CASE-1 results in enrichment function with comparatively steep gradient whereas CASE-4 produces a slowly varying function, while CASE-7 results in a relatively flatter enrichment function. To this end, in this study, only nine combinations of C and R_c are analysed for demonstration purpose. It is possible to systematically test even more combinations to further enhance the shape of the enrichment functions for best possible solutions. For the selected nine combinations, it is concluded that CASE-1 results in comparatively better shape of the enrichment functions that produce the lowest error for the considered problem.

5.2. Example problem 2

As a second example, we consider transient heat conduction problem in a two-dimensional domain $\Omega = [0, 2]^2$ with a heat source in the central part as shown in Figure 8. The heat dissipating source is $G = 200$ in the centre of the domain $(x, y) \in [0.8, 1.2]^2$ and is zero elsewhere. For numerical computations, the time step value is fixed at $\delta t = 0.001$ and computations are performed for 1000 time steps. The source dissipates heat during the whole of the simulation time. The convection heat transfer coefficient α and the heat diffusion coefficient λ are taken to be 1 and 0.1, respectively.

Example problem 2 assesses the effectiveness of the proposed error estimate for a more general problem where the analytical solution is not known. The L_2-norm error cannot be computed in this case and naturally an alternative indicator is needed to assess the accuracy of the numerical solution. The proposed error estimate is shown here to be used as a reliable indicator instead of the L_2-norm error. The purpose is to use the error estimate η for the selection the enrichment functions.

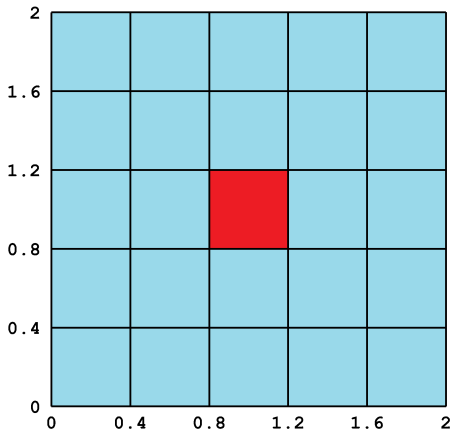

Figure 8: Domain configuration for Example problem 2 with a heat source (■) in the centre.

To investigate the effect of EF1 and EF2 enrichment functions on the solution of Example problem 2, we use a 5×5 mesh with different numbers of enrichment functions. Figure 9 shows the variation of η as a function of Q for both types of enrichment functions, at times $t = 0.2, 0.5$ and 1.0. As observed in the previous example, the value of η decreases with the increase of the number of enrichment functions. An interesting observation made from the results presented in Figure 9 is that for early simulation times EF2 enrichment functions perform better than EF1 enrichment functions, for the selected problem conditions. As the time progresses, results obtained with both types of enrichment functions become practically similar, see Figure 9(b). At $t = 1.0$ almost similar results are obtained with both types of enrichment functions. This suggests that if we want to solve the selected problem for a short time duration, then EF2 enrichment functions provide a better option because they efficiently capture the sharp thermal gradients at early simulation times. For long simulation times either EF1 or EF2 can be selected because both produce almost similar results. If we extrapolate the results, EF1 may perform better for much later time steps and it may become a more suitable option. If better accuracy is required at extended simulation times, EF1 will perform better because a higher number Q of

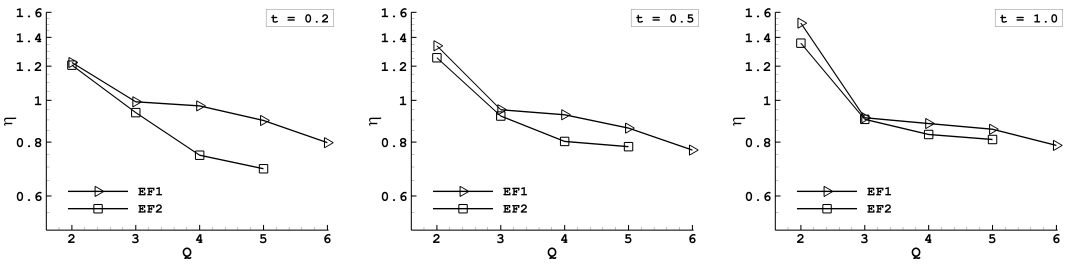

(a) (b) (c)

Figure 9: Variation of η with $q-$refinement for Example problem 2.

enrichment functions can be considered in comparison to EF1. From Figure 9(c), it is clear that better accuracy is achieved with EF1 using $Q = 6$. With EF2, we can use up to $Q = 5$ and the addition of a further enrichment function leads to the deterioration of the numerical results.

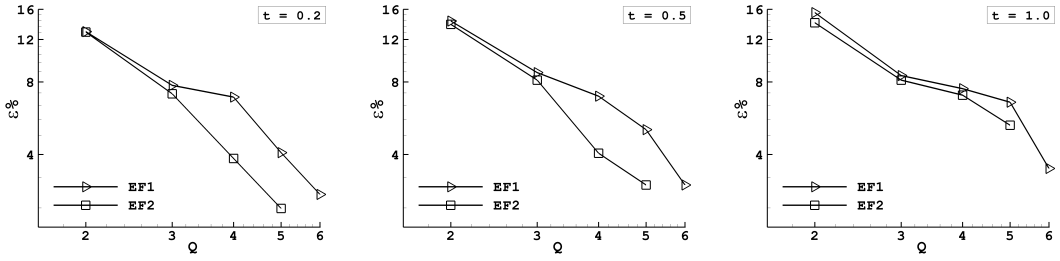

(a) (b) (c)

Figure 10: Variation of $\varepsilon\%$ with $q-$refinement for Example problem 2.

In the previous example, we established that the proposed error estimate behaves in a similar trend of the L_2-norm error, providing an upper bound, and for practical problems it can be used as an alternative tool to gauge the accuracy of GFEM approximations. In the current study we compute a reference solution using a very fine mesh with the standard FEM formulation to verify the accuracy of the error estimate. A preliminary study allowed to produce a reference FEM solution with 12,100 element mesh grid. As defined by (25), we calculate $\varepsilon\%$ where ϕ is calculated by GFEM approximation and Φ_{ext} is replaced by the FEM reference solution obtained with the fine mesh grid. Figure 10 depicts the values of $\varepsilon\%$ at three selected simulation times. It is clear from the figure that the accuracy assessed by $\varepsilon\%$ shows identical trends as that obtained by the proposed error estimate. At earlier simulation times, EF2 performs better than EF1 and at later simulation times almost similar values are obtained with both types of enrichment functions. Similar to the values of η with $Q = 6$ for EF2, the value of $\varepsilon\%$ also deteriorates with $Q = 6$ due to the relatively high condition numbers with EF2. The deterioration of the results of η and $\varepsilon\%$ for EF2 is depicted in Figure 11 at $t = 0.5$ and $t = 1.0$.

Table 4 presents the values of the condition number for EF1 and EF2 with increasing the number of enrichment functions Q. It is clear that consistently higher values of the condition number are experienced with EF2 compared to EF1. Using $Q = 2$ results in almost similar condition numbers for both enrichment functions. For higher values of Q, the difference in condition numbers for EF1 and EF2 increases, with the maximum difference observed with $Q = 6$. Again, in this example, the results deteriorate significantly once the condition number exceeds 1E+16. For EF1 the condition number, for $Q = 6$, is of the order 1E+13 while that for EF2 is of the order 1E+16, which leads to a large numerical error.

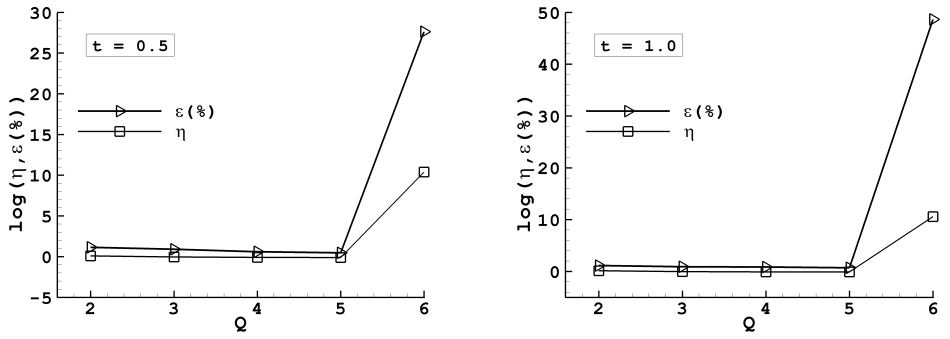

Figure 11: Variation of η and $\varepsilon\%$ with $q-$refinement for EF2 in Example problem 2.

Table 4: Condition Number (κ) with increasing Q for EF1 and EF2.

Q	κ(EF1)	κ(EF2)
2	1.46E+05	5.53E+05
3	2.53E+07	4.32E+08
4	4.30E+09	9.42E+11
5	5.12E+11	5.58E+14
6	1.64E+13	7.73E+16

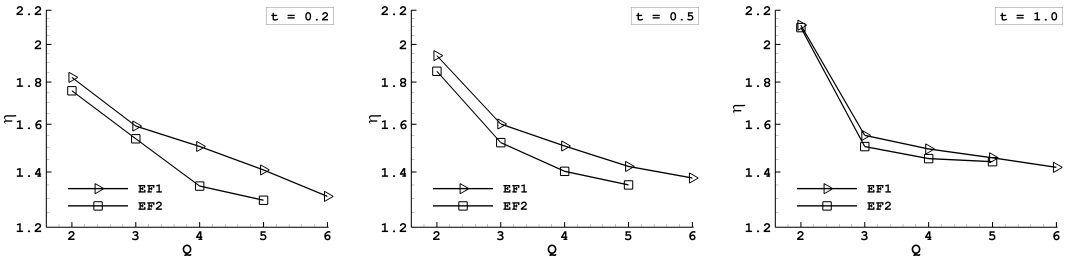

(a) (b) (c)

Figure 12: Variation of η with $q-$refinement for Example problem 3.

5.3. Example problem 3

The third example considers a problem in a three-dimensional domain in which the effectiveness of the proposed error estimate is tested for the selection of better enrichment functions. We extend the 2D problem considered in the previous section to a 3D domain $\Omega = [0, 2]^3$ with a symmetric heat source in the middle of the domain. The mesh density and all the physical parameters are also kept the same for the sake of consistency. We take a $5\times5\times5$ mesh with a heat source in the central part of the domain $(x, y, z) \in [0.8, 1.2]^3$ which dissipates heat at a constant rate $G = 200$ and is zero in the rest of the domain. The simulation time and time step value are also taken the same as in the previous example problem.

The purpose of Example problem 3 is not only to show the use of the proposed error estimate

for the selection of better enrichment functions, in a 3D domain, but it also shows that the error estimate does not depend on the scale of the problem. The error estimate is equally applicable to problems in 2D as well as in 3D domains. Figure 12 depicts a set of results at different simulation times showing similar trend to that obtained for the case of the 2D problem. At all the simulation times, a decrease in the value of η is observed with the increase in Q. As in the previous problem, comparatively better results are obtained with EF2 at early simulation times and almost similar results are produced at later simulation times by EF1 and EF2. In order to assess the accuracy of the approximate GFEM solution, we compute a reference FEM solution with a fine mesh grid, as in the previous example. We use a fine mesh of 216,000 elements to compute the reference solution and compare it to the GFEM solution by calculating $\varepsilon\%$ defined by (25). Again, producing reference solutions with very fine mesh grids is not a practical option for real-world problems. However, in the current study it is being used for verification purpose. For real-world problems, one can use our proposed error estimate as a tool instead of the L_2-norm error if no analytical solution is available. Figure 13 shows that similar trends of the results as captured by η, in previous considered cases, are also obtained by $\varepsilon\%$, verifying the accuracy of the proposed error estimate. For this 3D problem, the conclusions drawn from the results of the error estimate η are similar to those drawn from the previous results of the equivalent 2D problem.

6. Conclusions

In this work, a previously developed a residual *a-posteriori* error estimate is used for the selection of better performance enrichment functions for GFEM solutions of transient conduction heat transfer problems. Two types of enrichment functions are considered and their performance is tested in two-dimensional as well as three-dimensional problems. The first type of enrichment functions is based on *exponential* functions (EF1) while the second type is based on *sin* functions (EF2). Both enrichment functions mimic the solution behaviour and capture the heat diffusion

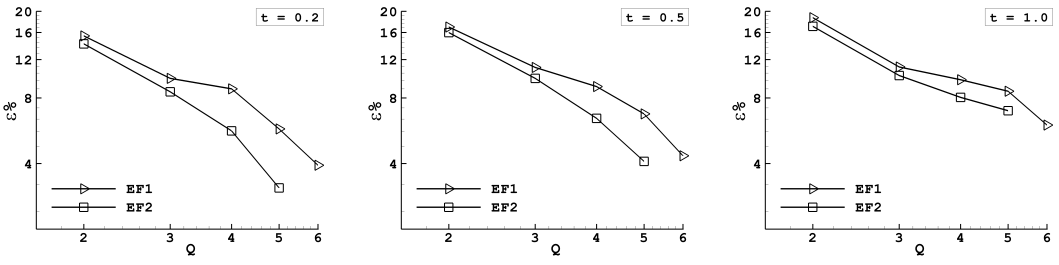

(a) (b) (c)

Figure 13: Variation of $\varepsilon\%$ with $q-$refinement for Example problem 3.

decay of the conduction heat transfer problems. To efficiently capture the time-dependent nature of the heat transfer, a multiplicity of enrichment functions of different standard deviations are used to enrich the approximation space. To test the performance of both enrichment functions, a residual *a-posteriori* error estimate is used as a tool to compute the discretization error of GFEM solutions when the number of enrichment functions is increased or the element size is reduced. The performance of both enrichment functions is tested on three numerical examples. The first example tests EF1 and EF2 for a problem with a known analytical solution and so both the relative L_2-norm error and the error estimate are computed. The results show that the type of enrichment functions influences the accuracy of GFEM solutions. It is also established that both the relative L_2-norm error and the error estimate behave in a similar way and lead to the same conclusion that EF1 performs better than EF2. The main emphasis of this study is to offer an effective tool which can effectively assess the performance of different enrichment functions for problems where analytical solutions are not available. For such problems, the computation of the L_2-norm error is not possible and so the error estimate can be used as an alternative reliable tool. For the considered problems, it is concluded that EF2 performs better at early simulation times while at later stages both EF1 and EF2 lead to practically similar results. The results of the three-dimensional problem lead to the same conclusions confirming that the error estimate effectively captures the solution trends and can be used as an effective tool for the selection of suitable enrichment functions for GFEM solutions of transient conduction heat transfer problems.

Acknowledgement

The first author is grateful for the Heriot-Watt University funding through a James Watt Scholarship.

References

[1] J. M. Melenk, I. Babuška, The partition of unity finite element method: basic theory and applications, Computer Methods in Applied Mechanics and Engineering 139 (1) (1996) 289–314.

[2] T. Strouboulis, I. Babuška, K. Copps, The design and analysis of the generalized finite element method, Computer Methods in Applied Mechanics and Engineering 181 (1) (2000) 43–69.

[3] T. Belytschko, T. Black, Elastic crack growth in finite elements with minimal remeshing, International Journal for Numerical Methods in Engineering 45 (5) (1999) 601–620.

[4] J. Dolbow, T. Belytschko, A finite element method for crack growth without remeshing, International Journal for Numerical Methods in Engineering 46 (1) (1999) 131–150.

[5] J. Chessa, T. Belytschko, An extended finite element method for two-phase fluids, Journal of Applied Mechanics 70 (1) (2003) 10–17.

[6] A. Gerstenberger, W. A. Wall, An extended finite element method/Lagrange multiplier based approach for fluid–structure interaction, Computer Methods in Applied Mechanics and Engineering 197 (19-20) (2008) 1699–1714.

[7] R. Merle, J. Dolbow, Solving thermal and phase change problems with the extended finite element method, Computational mechanics 28 (5) (2002) 339–350.

[8] M. Mohamed, M. Seaid, J. Trevelyan, O. Laghrouche, A partition of unity FEM for time-dependent diffusion problems using multiple enrichment functions, International Journal for Numerical Methods in Engineering 93 (3) (2013) 245–265.

[9] M. Iqbal, K. Masood, A. Aljuhni, A. Ahmad, Generalized finite element method with time-independent enrichment functions for 3D transient heat diffusion problems, International Journal of Heat and Mass Transfer 149 (2020) 118969.

[10] I. Babuška, U. Banerjee, J. E. Osborn, On principles for the selection of shape functions for the generalized finite element method, Computer Methods in Applied Mechanics and Engineering 191 (49) (2002) 5595–5629.

[11] I. Babuška, U. Banerjee, Stable generalized finite element method (SGFEM), Computer Methods in Applied Mechanics and Engineering 201 (2012) 91–111.

[12] T. Strouboulis, K. Copps, I. Babuska, The generalized finite element method: an example of its implementation and illustration of its performance, International Journal for Numerical Methods in Engineering 47 (8) (2000) 1401–1417.

[13] D. Turner, K. Nakshatrala, K. Hjelmstad, A stabilized formulation for the advection–diffusion equation using the Generalized Finite Element Method, International Journal for Numerical Methods in Fluids 66 (1) (2011) 64–81.

[14] I. Babuška, U. Banerjee, J. E. Osborn, Generalized finite element methods—main ideas, results and perspective, International Journal of Computational Methods 1 (01) (2004) 67–103.

[15] O. Laghrouche, P. Bettess, E. Perrey-Debain, J. Trevelyan, Wave interpolation finite elements for Helmholtz problems with jumps in the wave speed, Computer Methods in Applied Mechanics and Engineering 194 (2) (2005) 367–381.

[16] A. El Kacimi, O. Laghrouche, Numerical modelling of elastic wave scattering in frequency domain by the partition of unity finite element method, International Journal for Numerical Methods in Engineering 77 (12) (2009) 1646–1669.

[17] O. Laghrouche, M. Mohamed, Locally enriched finite elements for the Helmholtz equation in two dimensions, Computers & Structures 88 (23) (2010) 1469–1473.

[18] M. Drolia, M. S. Mohamed, O. Laghrouche, M. Seaid, A. El Kacimi, Explicit time integration with lumped mass matrix for enriched finite elements solution of time domain wave problems, Applied Mathematical Modelling 77 (2020) 1273–1293.

[19] C. A. Duarte, D.-J. Kim, Analysis and applications of a generalized finite element method with global–local enrichment functions, Computer Methods in Applied Mechanics and Engineering 197 (6) (2008) 487–504.

[20] T. Strouboulis, I. Babuška, R. Hidajat, The generalized finite element method for Helmholtz equation: theory, computation, and open problems, Computer Methods in Applied Mechanics and Engineering 195 (37) (2006) 4711–4731.

[21] T. Strouboulis, R. Hidajat, I. Babuška, The generalized finite element method for Helmholtz equation. Part II: Effect of choice of handbook functions, error due to absorbing boundary conditions and its assessment, Computer Methods in Applied Mechanics and Engineering 197 (5) (2008) 364–380.

[22] S. Langdon, S. N. Chandler-Wilde, A wavenumber independent boundary element method for an acoustic scattering problem, SIAM Journal on Numerical Analysis 43 (6) (2006) 2450–2477.

[23] E. Perrey-Debain, J. Trevelyan, P. Bettess, Wave boundary elements: A theoretical overview presenting applications in scattering of short waves, Engineering Analysis with Boundary Elements 28 (2) (2004) 131–141.

[24] R. Tezaur, C. Farhat, Three-dimensional discontinuous Galerkin elements with plane waves and Lagrange multipliers for the solution of mid-frequency Helmholtz problems, International Journal for Numerical Methods in Engineering 66 (5) (2006) 796–815.

[25] R. Tezaur, L. Zhang, C. Farhat, A discontinuous enrichment method for capturing evanescent waves in multiscale fluid and fluid/solid problems, Computer Methods in Applied Mechanics and Engineering 197 (19) (2008) 1680–1698.

[26] L. Zhang, R. Tezaur, C. Farhat, The discontinuous enrichment method for elastic wave propagation in the medium-frequency regime, International Journal for Numerical Methods in Engineering 66 (13) (2006) 2086–2114.

[27] O. Cessenat, B. Despres, Application of an ultra weak variational formulation of elliptic PDEs to the two-dimensional Helmholtz problem, SIAM Journal on Numerical Analysis 35 (1) (1998) 255–299.

[28] T. Huttunen, P. Gamallo, R. J. Astley, Comparison of two wave element methods for the Helmholtz problem, Communications in Numerical Methods in Engineering 25 (1) (2009) 35–52.

[29] T. Huttunen, P. Monk, F. Collino, J. P. Kaipio, The ultra-weak variational formulation for elastic wave problems, SIAM Journal on Scientific Computing 25 (5) (2004) 1717–1742.

[30] N. Sukumar, D. L. Chopp, N. Moës, T. Belytschko, Modeling holes and inclusions by level sets in the extended finite-element method, Computer Methods in Applied Mechanics and Engineering 190 (46) (2001) 6183–6200.

[31] V. P. Nguyen, T. Rabczuk, S. Bordas, M. Duflot, Meshless methods: A review and computer implementation aspects, Mathematics and Computers in Simulation 79 (3) (2008) 763–813.

[32] R. Simpson, J. Trevelyan, A partition of unity enriched dual boundary element method for accurate computations in fracture mechanics, Computer Methods in Applied Mechanics and Engineering 200 (1) (2011) 1–10.

[33] R. Simpson, J. Trevelyan, Evaluation of J_1 and J_2 integrals for curved cracks using an enriched boundary element method, Engineering Fracture Mechanics 78 (4) (2011) 623–637.

[34] W. Aquino, J. Brigham, C. Earls, N. Sukumar, Generalized finite element method using proper orthogonal decomposition, International Journal for Numerical Methods in Engineering 79 (7) (2009) 887–906.

[35] M. Malek, N. Izem, M. S. Mohamed, M. Seaid, O. Laghrouche, A partition of unity finite element method for three-dimensional transient diffusion problems with sharp gradients, Journal of Computational Physics 396 (2019) 702–717.

[36] M. S. Mohamed, M. Seaïd, J. Trevelyan, O. Laghrouche, Time-independent hybrid enrichment for finite element solution of transient conduction–radiation in diffusive grey media, Journal of Computational Physics 251 (2013) 81–101.

[37] M. S. Mohamed, M. Seaïd, J. Trevelyan, O. Laghrouche, An enriched finite element model with q-refinement for radiative boundary layers in glass cooling, Journal of Computational Physics 258 (2014) 718–737.

[38] T. Strouboulis, L. Zhang, D. Wang, I. Babuška, A posteriori error estimation for generalized finite element methods, Computer Methods in Applied Mechanics and Engineering 195 (9) (2006) 852–879.

[39] P. O'Hara, C. A. Duarte, T. Eason, Generalized finite element analysis of three-dimensional heat transfer problems exhibiting sharp thermal gradients, Computer Methods in Applied Mechanics and Engineering 198 (21) (2009) 1857–1871.

[40] P. O'Hara, C. Duarte, T. Eason, Transient analysis of sharp thermal gradients using coarse finite element meshes, Computer Methods in Applied Mechanics and Engineering 200 (5) (2011) 812–829.

[41] P. O'Hara, C. A. Duarte, T. Eason, J. Garzon, Efficient Analysis of Transient Heat Transfer Problems Exhibiting Sharp Thermal Gradients, Computational Mechanics 51 (2013) 743–764.

[42] M. Iqbal, H. Gimperlein, M. S. Mohamed, O. Laghrouche, An a posteriori error estimate for the generalized finite element method for transient heat diffusion problems, International Journal for Numerical Methods in Engineering 110 (12) (2017) 1103–1118.

[43] E. A. Munts, S. J. Hulshoff, R. De Borst, The partition-of-unity method for linear diffusion and convection problems: Accuracy, stabilization and multiscale interpretation, International Journal for Numerical Methods in Fluids 43 (2) (2003) 199–213.

[44] M. Iqbal, H. Gimperlein, O. Laghrouche, K. Alam, M. Shadi Mohamed, M. Abid, A residual a posteriori error estimate for partition of unity finite elements for three-dimensional transient heat diffusion problems using multiple global enrichment functions, International Journal for Numerical Methods in Engineering (2020) 10.1002/nme.6328.

[45] R. Lins, M. Ferreira, S. Proença, C. Duarte, An a-posteriori error estimator for linear elastic fracture mechanics using the stable generalized/extended finite element method, Computational Mechanics 56 (6) (2015) 947–965.

[46] H. Waisman, T. Belytschko, Parametric enrichment adaptivity by the extended finite element method, International Journal for Numerical Methods in Engineering 73 (12) (2008) 1671–1692.

[47] I. Babuska, R. Lipton, Optimal local approximation spaces for generalized finite element methods with application to multiscale problems, Multiscale Modeling & Simulation 9 (1) (2011) 373–406.